Fabrication of novel hybrid and mono magnesium base AZ31B/FlyAsh/TiC Nano-composite material via friction stir processing technique and improvement of mechanical tribological properties

Journal:	*Part E: Journal of Process Mechanical Engineering*
Manuscript ID	JPME-23-0134
Manuscript Type:	Original Article
Date Submitted by the Author:	07-Feb-2023
Complete List of Authors:	SAGAR, PREM; I K Gujral Punjab Technical University, Khanna, Sanjeev; University of Missouri, Mechanical Engineering Vignjevic, Rade; Brunel University, Structural Integrity
Keywords:	Metal Matrix Composite, Friction Stir Processing, Tensile Strength, Wear, Compressive Strength, Fly Ash, Magnesium, Microhardness, Nanohardness
Abstract:	The exceptional mechanical, microstructural, and tribological characteristics of friction stir processed (FSP) hybrid and mono nanocomposite materials resulted in growing research interest. In the presented work, the base matrix of magnesium-based AZ31B alloy was reinforced with Fly Ash (FA) and nano-TiC (n-TiC) particulates using FSP and resulting in both hybrid and mono composite surfaces. The microstructures and homogeneous distribution of reinforcing particulates of the synthesized composites were investigated with optical microscopy (OM) and field emission scanning electron microscopy (FESEM). In addition, for the synthesized nanocomposites mechanical and tribological characteristics were investigated including using tensile & compression strength, micro/ nano hardness, and wear characteristics. The OM and FESEM data indicate that owing to the significant impact of the FSP process, grain refinement and the homogenous dispersion of the FA and n-TiC nanoparticles for both mono and hybrid composites were achieved. Overall, the new Nano-hybrid composites have better mechanical properties due to improved interfacial bonding and homogeneous dispersion of hybridized n-TiC/FA reinforcements. The results indicate

	that AZ31B/FA/TiC hybrid nanocomposite has better mechanical and tribological characteristics than the base alloy and the mono composite materials. More specifically, the grain size was reduced nearly 20 times, microhardness was 1.72 times higher, ultimate tensile strength (UTS) was 2.42 times higher, compressive strength was 2.57 times higher, and wear rate was, about 80% higher when contrasted to the base alloy.

Title Page

Fabrication of novel hybrid and mono magnesium base AZ31B/FlyAsh/TiC Nano-composite material via friction stir processing technique and improvement of mechanical tribological properties

Author-

Dr. Prem Sagar1*
Department of Mechanical Engineering
The Technological Institute of Textile Sciences,
Bhiwani, Pin/Zip code-127021
Haryana
India-**+91**
E-mail- jasujaprem@gmail.com
Mob-+91-8295432672

Co-Author

Prof Rade Vignjevic2
Mechanical and Aerospace Engineering
Brunel University London, UK
Kingston Lane
Uxbridge
Middlesex UB8 3PH
E-mail: v.rade@brunel.ac.uk
Tel: +44 (0)1895 268455

Co-Author

Prof Sanjeev Khanna3

Mechanical & Aerospace Engineering, University of Missouri
W1024 Lafferre Hall
Columbia, MO 65211
USA
Phone: 5738849109
Email: khannas@missouri.edu

Declaration of interests

☒ The authors declare that they have no known competing financial interests or personal relationships that could have appeared to influence the work reported in this paper.

Corresponding Author- jasujaprem@gmail.com

Fabrication of novel hybrid and mono magnesium base AZ31B/FlyAsh/TiC Nano-composite material via friction stir processing technique and improvement of mechanical tribological properties

Abstract:
The exceptional mechanical, microstructural, and tribological characteristics of friction stir processed (FSP) hybrid and mono nanocomposite materials resulted in growing research interest. In the presented work, the base matrix of magnesium-based AZ31B alloy was reinforced with Fly Ash (FA) and nano-TiC (n-TiC) particulates using FSP and resulting in both hybrid and mono composite surfaces. The microstructures and homogeneous distribution of reinforcing particulates of the synthesized composites were investigated with optical microscopy (OM) and field emission scanning electron microscopy (FESEM). In addition, for the synthesized nanocomposites mechanical and tribological characteristics were investigated including using tensile & compression strength, micro/ nano hardness, and wear characteristics. The OM and FESEM data indicate that owing to the significant impact of the FSP process, grain refinement and the homogenous dispersion of the FA and n-TiC nanoparticles for both mono and hybrid composites were achieved. Overall, the new Nano-hybrid composites have better mechanical properties due to improved interfacial bonding and homogeneous dispersion of hybridized n-TiC/FA reinforcements. The results indicate that AZ31B/FA/TiC hybrid nanocomposite has better mechanical and tribological characteristics than the base alloy and the mono composite materials. More specifically, the grain size was reduced nearly 20 times, microhardness was 1.72 times higher, ultimate tensile strength (UTS) was 2.42 times higher, compressive strength was 2.57 times higher, and wear rate was, about 80% higher when contrasted to the base alloy.

Keywords: Hybrid nanocomposite, FSP, Microstructure, Micro hardness, Fly Ash

1. Introduction:

Demand and search for materials with improved surface qualities including mechanical and tribological properties is steadily increasing. Composite materials are worthy candidates because of their exceptional qualities, high specific strength, and refined microstructure. A significant amount of research is going towards the enhancement of Magnesium based composite materials by using reinforcement additions [1, 2]. In this regard, properties like low density, electromagnetic shielding effectiveness, and lower energy consumption during production make magnesium (Mg) a vital material in substituting conventional materials like steel and aluminum. For instance, the North American automotive strategic vision for magnesium (NAASVM-2020), states that in a mass reduction scenario 100 kg of Mg can replace 200 kg of steel, while 45 kg of magnesium can replace 65 kg of aluminum [3]. In spite of these advantages, the low hardness, elastic modulus, inferior resistance to wear, and flammability risks of magnesium alloys restrict the extensive use of these lightweight alloys in structural applications [4-6]. Recent research shows that synthesizing new magnesium metal matrix composite (MMMC) by incorporating secondary phase particulates, can enhance mechanical and other characteristics of base Mg alloy [1]. However, a number of studies also demonstrate the possibilities to use two different kinds of reinforcement particulates in development of hybrid composite materials [2, 7-8]. Due to these favorable qualities, MMMCs

are regarded as a material that might compete with aluminum based composites [9, 10]. However, MMMCs are more expensive to produce than composites made of aluminum [11]. Production costs can be decreased if industrial discarded constituents are efficiently utilized as reinforcing particles for MMMCs [12]. One of the materials that have the potential to be used as reinforcement is fly ash (FA). It is a type of industrial waste that results from coal burning in thermal power plants. It is removed from the exhaust gas by appropriate filtration techniques. It is readily available all over the world and can be used to strengthen MMMCs without endangering the environment by causing land contamination. Solid precipitator and hollow cenosphere shells form the two categories of FA. The main components of FA are aluminum oxide (Al_2O_3), silicon oxide (SiO_2), and calcium oxide (CaO) [13]. By adopting the friction stir processing technique, Kondaiah et al. [14] created an AZ31/FA MMC and achieved improved mechanical and wear properties. Also, the improvement in the mechanical characteristics of the as-cast alloy was reported in [15]. In this study, the wastes like FA and red mud were used as reinforcement. Additionally, it has been shown that hybrid surface composites with reinforcement of two or more nanoparticle types can affect the way base alloys or mono composites perform [2, 7]. One of the most advanced methods employed in the creation of a hybrid composite matrix is the friction stir process (FSP). Unlike other methods, FSP allows for use of wide range of powders. Many researchers adopted the FSP technique to incorporate different secondary phase particulates such as SiC [16], Al_2O_3 [17], TiC [18], and CNT [19] into magnesium alloys.

In the current study, n-TiC (average particle size 80 nm) and FA (particles in micron size) were used as reinforcement nanoparticles. The AZ31B/TiC/FA hybrid surface composite and the AZ31B/TiC, AZ31B/FA mono nanocomposite were prepared using FSP to investigate the hybrid impact of those nanoparticles. The microstructure, mechanical and tribological characteristics were examined by various testing methodologies and FESEM.

2. Experimental method

2.1 Materials

For the development of mono and hybrid composites magnesium, alloy AZ31B was used as the base matrix. Different plates of AZ31B with dimensions 250× 100× 6.3 mm were used for the final experiment characterization. To examine and validate the content of Mg and other constituents of, as received, AZ31B Mg alloy was determined by FESEM- Energy-dispersive spectroscopy (EDS). FESEM-EDS analysis, (as shown in **Supplementary Figure 1a**), confirmed the presence of Mg as the major element and various other elements with evidence of no carbon content. The elemental constitution of the base Mg (AZ31B) matrix is presented in **Supplementary Table 1**. For mixing up of the reinforcement into the base metal and fabricating new mono and hybrid composites via FSP process, blind holes with 2 mm diameter and 4mm depth were drilled over the top surface of base AZ31B Mg plates, as shown in **Supplementary Figure 1(b).**

2.2 Reinforcements Used

Nano titanium carbide (n-TiC), has impressive properties like high hardness and resistance to oxidation. The n-TiC particulates with an average 80nm size and 99.99% purity were used as secondary phase reinforcement particulates. FESEM, EDS, and X-ray diffraction (XRD) patterns for the n-TiC reinforcement are shown in **Supplementary Figure 2 (a, b, and c)**. **Supplementary Table 2** presents the weight along with the atomic percentage of nano TiC reinforcement particles. The second type of reinforcement was FA which was obtained from the coal-fired steam generating plant Bhiwani textile mill, (Bhiwani) India. The SEM analysis showing the average particle size and morphology for the FA particulates is presented in **Supplementary Figure 2 (d).** However, the EDS analysis result showing particle contents is presented in **Supplementary Figure 2(e),** which clearly shows the presence of Silica and other FA constituents.

2.3 Fabrication of mono and hybrid nanocomposite materials

The reinforcement particles were introduced to the blind holes of the AZ31B base matrix by the FSP technique to manufacture mono and hybrid composite. The FSP process (as shown in **Supplementary Figure 3**) was carried out on a dedicated computer numeric control vertical milling center. The FSP process comprises two stages. First – sealing of the holes filled with the reinforcement particulates is performed with the pin less tool. Second – mixing of the reinforcement into the matrix material which is performed with the tool with a pin. To exclude the presence of any material defect, a pilot study was conducted aiming to choose the optimal set of parameters along with the tool profile. Two tools (with a pin less shoulder and a taper cylindrical pin profile) made up of high carbon high chromium (HCHCr) steel were selected after the pilot study. This selection was made since the samples manufactured using these tools revealed no flaws. The tool without a pin was only used to seal off the top cover of the holes after incorporating n-TiC and FA particulates for mono composite and TiC/FA for hybrid composite fabrication. The tool with a taper cylindrical pin profile with a shoulder diameter of 16 mm and a pin length of 4 mm, is shown in **Supplementary Figure 4**. Final manufacturing was performed with the tool revolution speed of 1800 rpm, the tool transverse speed of 20mm/min and three FSP passes to consolidate reinforcement into the Mg base alloy. Following the FSP procedure, the various manufactured surfaces are shown in **Supplementary Figure 5.** It, depicts the typical crown appearance of developed surfaces fabricated via FSP process. The crown appears smooth, devoid of prominences or depressions. There are semicircular characteristics that resemble those produced by standard milling. Hence it is justified that process parameters are adequate to generate a crown with no flaws. In order to comply with the ASTM standards for testing and analysis the fabricated samples underwent different preparation processes. In the case of hybrid surface composite, 50% of n-TiC and 50% of FA reinforce particles were mixed (by volume %) for filling up the volume of the blind holes. The mono composite surfaces were manufactured by adding n-TiC and FA reinforcement particulates separately, before applying the final synthesis process by FSP.

2.4 *Microstructural characterization*

Standard metallographic approaches were used after the mono and hybrid nanocomposites were synthesized. The metallographic specimen was cut perpendicular to the stir zone (SZ) of FSP. After that, the obtained specimen was grounded polished, and etched with the picric acid etching solution. Further OM and JEOL USA FESEM equipped with EDS FESEM which were used to characterize the microstructure, interface bonding, and homogenous distribution of reinforcement.

2.5 Mechanical testing

The prepared specimens were tested for microhardness, nanoindentation, tensile test, and compressive strength. According to ASTM guidelines, the Vickers hardness method was employed to quantify micro-hardness. A 15-second dwell period was used with a 500 g load at 0.5 mm indentation intervals. Each indentation site received three measurements, and the average of these readings was used as the final value. The nano-hardness was measured using a Hysitron triboindenter, equipped with a Berkovich diamond three-sided pyramid tip in a quasi-static indentation mode, having a radius of curvature of 150nm. At a peak load of 500 mN, an indentation was created on the polished surface of specimens with a fixed loading time of 10 s and unloading time of 2s and up to 20µm. The value of nano hardness was calculated utilizing equations given in [20].

In order to perform tensile and compression testing on the base, mono composites, and hybrid composite, specimens from the stir zones of each fabricated composite were extracted using Wire cut electric discharge machine (WEDM), in accordance with ASTM E-8 M and ASTM E-9 standards (please see **Supplementary Figure 6).** A Tinius Olsen UTM (model HKS50) with a load capacity of 50 KN and an initial strain rate of $1 \times 10^{-4\,s^{-1}}$ was used to examine the ultimate tensile and compressive strength of each specimen type. In the nanocomposites and the base Mg alloy samples the crack nucleation sites and crack propagation were further examined using FESEM, after final breaking.

2.6 Tribological properties Tests

WEDM was used to extract pins with a size of 3 mm x 30 mm from base metal and composite materials in order to study wear and friction characteristics. A pictorial view of the extracted specimen for the wear test is given in **Supplementary Figure 7.** Every experiment adhered to ASTM G99 standards and was assessed using a pin-on-disc tribotester (DUCOM TR-20 LE). A sliding distance of 700 m, a time period of 300 s, a disc rotational speed of 400 rpm, and a fixed load of 20 N was used in all wear studies. The final loss of height values was multiplied by the pin's cross-sectional area to determine the volumetric loss. The final wear rate was obtained by dividing volumetric loss by sliding distance. Wear morphology was examined using FESEM.

3. Results and Discussion

A typical stir zone (SZ) crown is shown in **Supplementary Figure 5** for the FSPed mono and hybrid composite materials. The crown's surface is completely flat, free of any voids and discontinuities. The texture of the crown includes semi-circular striations that were created by the rotating tool rubbing against the surface. Weld pitch, which is the ratio of traverse and tool rotational speeds, is proportional to the distance between the striations [21].

3.1 Micro-structural characterization

The microstructural characterization of AZ31B Mg matrix alloy and the fabricated mono and hybrid nanocomposite was successfully examined by a trinocular inverted metallurgical microscope and at different magnifications. All the micrographs captured are presented in **Figure 1**. It is noticeable from **Figure 1 (a)** that the microstructure of AZ31B base magnesium alloy is characterized by coarse α-Mg and β-Mg_{17}-Al_{12} and possesses a discontinuous network at the grain boundary. Unrefined coarse grains were observed in a distributed manner for the base metal matrix. In addition to that, alongside segregated large crystals, clusters of tiny crystals were also present. The magnesium base AZ31B alloy had an average grain size of 78 µm. As presented in **Figure 1 (b-d) i.e.** Stir zone micrographs of the mono and hybrid composite show refined grain structure. Microscopy images demonstrated that coarse magnesium grains were broken and refined by the action and rotation of the FSP tool. The findings of the stir zone reveal the presence of dynamic recrystallization as a leading phenomenon. Where the material had undergone intense plastic deformation like stir zone, a high degree of grain refinement was observed. In addition to the above high thermal energy produced by FSP rotating tool, causes dynamic recrystallization which has as a consequence the evolution of fine grains, similar to what was reported in [22, 23]. For all manufactured composites, this frictional heat is further liable for the refining of the grains in the stir zone, which is also in agreement with [24]. For both mono and hybrid composites, the refined microstructure is due to grain boundary pinning with reinforced particulates. Also, the multiple passes resulted in the increased level of stirring and reduced the asymmetry in the structure of the FSP zone caused by the asymmetric material flow produced by the tool rotation and traverse motion. This resulted in the homogenous distribution of reinforcements with fine grains which is in agreement with [25]. Lastly, n-TiC and FA both resisted grain growth in the case of both mono and hybrid composite materials, owing to the peening effect caused after dynamic recrystallization, as it prevents the migration of grain boundaries and restricts grain growth after FSP. In addition, these secondary phase particulates act as heterogeneous nucleation sites for magnesium grains and lead to finer grain structures, also in agreement with [25]. Average grain size values of the base, mono, and hybrid composite materials are presented in **Table 1.**

The FESEM result of the mono and hybrid composite specimens are shown in **Figure 2**. From the comparison of microstructure and FESEM results (as presented in **Figure 1** and **2**) of the base and

composite materials, it is confirmed that large crystals, during loading, break down into smaller ones and increases the area of stress concentration, which is prone to initiate cracks during loading. It is evident from **Figure 1 (b-d) and Figure 2** that the region of stress concentration has grown as a result of the breakdown of larger crystals into smaller ones, making it more likely to crack under load. As a result, the need for secondary reinforcement particles is legitimate. For instance, in AZ31B/TiC mono composite the n-TiC particles represent obstacles and constrain the movement of dislocations. In addition, FSP fragments the larger intermetallic particles into smaller ones and redistributes them throughout the matrix with more uniformity. The FA particle distribution for AZ31B/FA mono composite is shown in **Figure 2**. This distribution may be attributed to action of the FSP tool and the related plastic flow which may have fragmented the large reinforcement particulates and changed their size and morphology, which is also reported in [26]. These small sizes particulates, the Cenosphere of FA, are redistributed in the base matrix in a homogenous manner. The lack of clustering of debris from the fragmentation of the particulates indicates that fragments continued to mix with the plasticized metal and were uniformly distributed throughout the matrix. The dispersion of reinforcement within the magnesium alloy matrix depends on the speed at which the tool rotates [24], which in current research work is good enough.

3.2 Mechanical Characteristics

3.2.1 Microhardness and Nano-indentation

The micro hardness of the mono and hybrid composite materials was measured relative to the stir zone region. All the measured values are given in **Table 1** and represented graphically in **Figure 3.** The graph shows that the microhardness of the hybrid AZ31B/TiC/FA (95.1 Hv) is significantly higher than the microhardness of the base AZ31B Mg alloy (55Hv), the nanocomposites AZ31B/TiC (89.2) and AZ31B/FA (80.1).

The increase in microhardness is the consequence of the microstructure change resulting from FSP and reinforcement by the n-TiC/FA particles. And as per the Hall-Petch equations, microhardness increases as grain size decreases [27]. Therefore, it can be claimed that smaller grain boundaries cause increased microhardness. In the case of AZ31B/TiC mono composite, the possible cause of enhanced microhardness is the ability of nano-sized reinforcements to restrict grain boundary movement. This is in accordance with the Zener pinning effect, and the strengthening of grain boundary which is in compliance with the well-known Hall-Petch equation [27]. In the case of AZ31B/FA mono composite, in addition to the Hall-pitch and Orwan hardening mechanisms, the reduction in the average inter-particle distance caused by the FA particle fragmentation contributed to the enhanced microhardness. For hybrid composite, the possible cause of the high value of microhardness is the presence of different sizes of reinforce particulates i.e. nanoparticles for n-TiC and microsize particles for FA, which results in good dispersion, which further enables reinforcement to settle well around the grains during the recrystallization process and leverage microhardness properties. Lastly, different degrees of dislocation density was created in the composites due to temperature difference between FA particulates and the base Mg metal matrix,

causes a quench hardening effect.. In addition to the above, for all fabricated composite materials three FSP passes reduce the composite's surface area, which further decreases the inter-particle spacing in the SZ and increased the microhardness, which was also reported in [28,29]. The results presented in the previous section in order to illustrate enhancement of hardness of the composite materials can be further supported by the force displacement curves from the Nano-hardness tests shown in **Figure 4**. It is obvious that the load-displacement curve (as it shift leftwards) for hybrid AZ31B/TiC/FA composite indicates lowest depth of indentation, i.e. highest hardness. This might be due to the excellent pulsating action provided by the tool pin which helps for better dispersion of nano reinforcement particles during FSP in SZ that is responsible for higher hardness values. Also, the better distribution of reinforcement particles at high heat input resulted in the formation of small grain size. This small-size grain development is accountable for higher hardness.

3.2.3 Tensile experiments

Supplementary Figure 8 shows the tensile and compressive specimen before and after the experiments which were performed according to ASTM standards. In comparison to base metal, both mono and hybrid composites displayed better strength and ductility values presented in **Table 2**. According to **Table 2**, all specimens achieved higher UTS and strain at failure when compared with the base magnesium metal matrix. The modulus of elasticity, UTS and yield strength (YS) of the synthesized composites were significantly increased by the introduction of secondary phase particulates when compared to the base AZ31B Mg matrix as shown in **Figure 5**. The base material's lower UTS is a result of its coarse grain and the presence of Mg precipitates at grain boundaries. As a result, these precipitates become ideal locations for fracture initiation. Due to the reduced grain bonding strength caused by these Mg precipitates, crack initiation and propagation are more likely to occur near to these precipitates. The tensile property enhancements are a consequence of microstructural modifications brought on by processing, such as grain refinement, resistant to dislocation dispersion in the matrix, and reinforcement-matrix interaction [30]. The reduced average grain size values are presented in **Table 1**, which clearly shows significant grain refinement and homogenous dispersion of dislocations in the matrix, which corresponds to the enhancement of properties from the base AZ31Mg matrix to the hybrid composite. The higher UTS value of hybrid composite as compared to base alloy and mono composites, and high UTS value of mono composites as compared to base alloy is might be due to the smaller grains. The refinement of the grain size in the specimens increased the density of the available boundaries, which can efficiently cause obstacles to the movement of dislocation and in turn increase the strength. The mono-composites exhibited higher yield stress, strain to failure, and lower plastic hardening rate than compared the base Mg alloy. The hybrid composite exhibited higher yield stress and higher plastic hardening rate than compared the base Mg alloy and the mono-composites. For AZ31B/TiC mono composite the introduction of the hard n-TiC particulates and the refinement in the grain size improved elastic stiffness (higher elastic modulus) and increased the tensile strength by shifting the load from the magnesium matrix to the hard reinforcements,

which is in agreement with [30]. Additionally, the dispersion of nano-reinforcements resulted in an increase of the material's elasticity moduli. For instance, TiC's high elastic modulus and strong interfacial interaction with the matrix were prime reason of increases in elastic modulus. The distribution of particulates along the grain boundaries of the developed hybrid AZ31B/FA/TiC is the cause of the load transfer from the ductile magnesium phase to the hard-brittle phases. And especially for mono composite AZ31B/FA the FA particles have a significant wettability that enables load distribution and transfer from the base matrix to the reinforced particulates, hence strain to failure was significantly increased for all composites.

3.2.3.1 Fractography

The location of crack onset and the fracture mechanism present in the samples from the tensile tests of the nano-composite and the monolithic A31B alloy were investigated using FESEM fractography. A typical tensile fracture surface was present in all samples, see **Figure 6**. **Figure 6(a),** illustrates the development of cracks in monolithic AZ31B magnesium alloy. Monolithic Mg fractures via a cleavage mode of fracture as a result of the lack of homogeneity (brittle fracture). Mg deforms as a result of a restricted basal slip. This might have been caused by the tensile test-induced crack propagation from weaker surfaces, which the Griffith theory of failure also covers nicely [32].

Figure 6 (b), represents the fracture mode of AZ31B/FA mono composite. Micro cracks in the fractured surfaces of nanocomposite samples during the tension test are an indication of the brittle deformation of nanocomposites. These cracks may arise due to less strong bonding of reinforcement and the base matrix. A small void is also visible on the fractograph. In general, debonding, particle pull out, and matrix cracking—which may happen as a result of overloading—are attributed to voids. As noted by Sun, S.et al., [33], the general rule is that the existence of voids directly affects the elongations of the material during tensile testing. The fracture mode may also be gradually shifting toward the brittle mode, according to a rise in surface flatness, which is consistent with Thangarasu A et al [28]. Additionally, to support the aforementioned claim that rosette patterns resulted in honeycomb dimples, it should be noted that the material's quasi-cleavage suggests a mode of fracture between ductile and brittle. The fracture mechanism of the AZ31B/TiC mono composite is shown in **Figure 6 (c).** The increased fracture surface flatness caused by the inclusion of n-TiC particles also comes from the reduced material flow brought on by improved strengthening. As was already noted, it was found that the bulk of the nano titanium carbide particles was enmeshed in the base matrix. The matrix and the substance containing the n-TiC (hard inclusions) did not deform at the same pace, it was also found. In order to resolve this disparity, nucleation of voids was reported. The n-TiC particles fracture as a result of this nucleation, which also causes the sites at the particle-metal interface to split. The nucleation may cause the inclusion to fracture or the inclusion-matrix interface to lose cohesion. The base matrix was discovered to be embedded with n- TiC reinforcement particles, which leads to ductile failure

of the composites. In addition, the combined influence of basal and non-basal slip produced by nano-size reinforcements causes the fracture mode of Mg nanocomposites to change from pure Mg in most situations to a ductile fracture. In **Figure 6 (d),** the dimple structures that could be clearly observed in the hybrid AZ31B/FA/TiC composite were finer and more intensive than those in the base and mono composites. The lack of micro cracks and voids is a clear indicator of the large plastic deformation of nanocomposites. These dimples type features are more distinguished in nanocomposite materials fractography, which clearly indicates that these nanocomposites hold enhanced ductility. In comparison to monolithic material, the majority of reinforced magnesium nanocomposites demonstrated strong microcrack formation resistance and minimal tensile cavitation. The grain boundary's ability to prevent dislocation movement and deformation also gave the hybrid composite substantially greater strength and elongation than the other composites. Although there were a few ash particles that weren't totally broken, they were minimal. On the tensile strength and elongation, they had no appreciable impact. Therefore, it was determined that three FSP passes greatly increased the tensile strength and elongation of the hybrid composite. Also, the presence of tear edges around little dimples also shows the ductile nature of the fracture. Lastly, it can be seen from **Supplementary Figure 8**, that base monolithic Mg shows brittle (flat) fracture type, however, tensile test failures for the composites happened at a nearly 45-degree angle to the tensile loading axis, which clarified that the mode of fracture shifts to ductile (shear) fracture, which is in agreement with [34].

3.2.3.2 *Compression experiments*

Compression test results for base Mg alloy, mono AZ31B/TiC, mono AZ31B/FA and hybrid AZ31B/FA/TiC composite in the form of the stress-strain plot are presented in **Figure 7** and corresponding values are tabulated in **Table 3**. From **Figure 7**, it is clear that fabricated composite materials do possess a high value of yield strength and ultimate compressive strength (UCS). For magnesium, twinning is the most favorable deformation phase under compressive stress. The activity and spread of twinning in pure Mg occur favorably and unhindered by factors like the existence of secondary phases or coarse grain size. Twin activation and propagation may be challenging in the case of composites because of limitations posed by reinforcement and grain refinement. The yielding of pure Mg at low strengths can be explained by easy twin nucleation, whereas the yielding of composites at high strengths is correlated with delayed twin activation. Pure Mg showed increased failure strain as a result of the facile twin propagation. Barriers in composites, such as second phases and more grain boundaries, prevented twin propagation. Thus, when the continuity of twinning stopped, the composites failed at lower failure strain. In general, the resulting failure mechanisms in pure Mg and its composites are consistent with findings from earlier studies [35]. This clearly indicates that adding secondary phase particulates and the FSP process directly contributes to leverage compressive strength properties. It may be attributed to the pinning effect cussed by secondary phase particulates and high heat developed by the FSP tool, which straight away causes grain refinement and formation of participates phase, which further contributes in improving the micro-hardness and strength of the material. Smaller crystals are produced as a result of the larger original grain structure shattering during the FSP, which increases

the stress concentration area and causes the material to fail upon loading. The secondary phase reinforcing particles' involvement limits the mobility of dislocations and aids in the composite strength [35]. In the present case, the reinforced particulates that must be mixed with the AZ31B base alloy in order to prevent the gliding of dislocations in the stir zone are nano-reinforcements like n-TiC, FA, and hybrid compositions of both. Therefore, as compared to the base AZ31B Mg, additional stress is needed to overcome the interplay of dislocation and restriction, which increases the strength of the composite. Later, dislocation avoids the particulates by bending through the sidewalls during loading, the motion occurs in a loop shape and is known as Orowan looping around the secondary phase particles. These loops might result in back stress, which limits the deformation up to a higher strain value and composite strength. With additional nano reinforcement particulates engaging in the stir zone, which results in delayed crack nucleation and propagation, the compressive fracture strength of the hybrid nanocomposite has risen up to 1.88 times, indicating a rise in the ease of slips [36]**.**

3.3 Wear mechanism

Wear rate values for the fabricated composite materials as well as the base material are presented in **Supplementary Table 3.** Also, the progressive height loss value for the developed composite as well as the base magnesium material is presented in **Supplementary Figure 9.** Lower wear rate values for the hybrid composite material and titanium carbide base mono composite material might be attributed to the high micro-hardness values. Also, as per Archard's wear law [37], the hardness of metallic materials has an inverse connection with the wear rate. All the mono, as well as hybrid, develop composite materials possess a lower value of wear rate as compared to the base material. The improved toughened surface efficiently sustains the counterforce asperities' cutting action. Additionally, the developed composite has a lower coefficient of friction (COF), all corresponding values of COF are also given in **Supplementary Table 3.** Homogenous dispersion of the reinforced particles leads to minimizing the interaction zone between the sliding pin and the counter face plate. The titanium carbide and FA particulates in the mono and hybrid composites provide adequate support for the imposed load. Lower values of COF further lead to a reduction in the acting shear stress on the sliding surface which consecutively helps in developing improvements in the wear resistance. Owing to the Hall-pitch mechanism which contributes to the evolution of grain boundary and pinning of secondary during FSP, also contribute to the formation of composite hardness and strength which further result in an improved force bearing competence and decreased wear rate.

3.3.1 Wear fractography

Through SEM analysis, worn Surface morphology was examined. **Supplementary Figure 10** shows SEM images of all specimens processed using FSP and base AZ31B alloy. It was noted from **Supplementary Figure 10 (a)** that the underlying material AZ31B has a texture made up of deep, straight ploughs. This might be caused by the as-manufactured Mg network, like - Mg17Al12, being heated up by friction, and showing an inability to withstand this much of thermal energy and consequently break down easily. The material softened as a result of this brittle and coarse phase's ineffectiveness to function as an obstruction to wear. These deep grooves were principally caused by the predominance of the abrasive wear process. It ultimately caused wear

debris to accumulate over the base metal's texture. Additionally, the morphology of the base AZ31B monolithic Mg worn-out surface revealed considerable plastic deformation and detachment of material from the primary Mg base matrix. This might also be a result of higher growth in heating values due to intense friction. The material's substantial plastic deformation and separation from the basic Mg matrix further supported the idea that this sample had delamination wear along with an adhesive wear mechanism. This might be explained by the material's lower softness when compared to FSPed composites. Primary monolithic Mg alloy showed a range of adhesive and abrasive wear, also as in consensus with Madhusudhan Reddy et al. [38].

The composites' wear component, however, was different from that of the basic metal. Homogenous and uniform dispersal of n-TiC particles have an impact on wear resistance. The inclusion of n-TiC particles also caused a change from severe to mild wear by decreasing the amount of metal-to-metal contact area and the direct load. On the other hand, AZ31B/TiC as shown in **Supplementary Figure 10 (c),** specimen demonstrated the supremacy of a minor abrasive wear mechanism by having shallow grooves and fewer pits along the wear paths. The magnesium alloy composite's wear morphology may have been caused by the n-TiC particles being pulled out of the material. Abrasive wear was the primary cause, as evidenced by the existence of loose debris particles on almost every surface of composites that had been created. The primary contributors to the appearance of these loose debris bits are sliding n-TiC tugging and oxidizing mono composite. The progress of constant friction was also the main cause of the change of the worn surface from scratches to grooves. Mild abrasive and wear debris production, as well as the occurrence of a delamination wear mechanism, were observed for the AZ31B/FA specimen as shown in **Supplementary Figure 10 (b).** This delamination wear phenomenon may be mostly attributable to shear plastic deformation, which caused fractures to form and spread under the surface. These cracks ultimately cause layered areas to separate, as in tune with Sarmadi et al. [39]. The buildup of dislocations under the surface is chiefly accountable for the development of pores in the subsurface region. The interface between particles and magnesium alloy might develop pores since there were no chemical bonds between them. Cracks start to appear as a result of pores combining, and as they continue to grow as wear occurs, wear debris is produced. Due to the superior nanoparticle distribution in AZ31B/FA/TiC hybrid composite. The specimen had a surface with fewer micro cracks, as shown in **Supplementary Figure 10 (d**). Additionally, this consistent distribution not only avoids delamination but also the immediate contact load.

Conclusions:

Successful fabrication of composite materials (hybrid and mono) was accomplished utilizing FSP. To strengthen, the n-TiC and FA Nanopowder were utilized to reinforce AZ31B magnesium wrought alloy. The following findings were made as a result of this.

The outcome of the study reveals that grain sizes of the developed composites were reduced by 10 times as compared to parent AZ1B alloy, demonstrating the significant impact that FSP has on grain refining. Additionally, by changing the grain from coarse and elongated grains to finer and equiaxial grains, grain aspect ratio was enhanced. Due to the incorporation and fusion of the n-TiC

and fly ash (FA) reinforce particles during the fabrication process, the hybrid AZ31B/TiC/FA nanocomposite showed a worthier outcome in mechanical, wear characteristics, and microhardness behavior. Furthermore, attributed to differences in reinforcement nanoparticles characteristics and particle sizes, impressive, homogenous, and uniform dispersal of the nanoparticles for reinforcement was accomplished. On the other hand, owing to the inclusion of ceramic nanoparticles in the manufactured surface reduced the strain rate of the hybrid and mono composite matrix, improving the UTS stress of the hybrid composite by around 70% compared to the alloy as received.

References:

1. Sagar P, Handa A, Kumar G. Metallurgical, mechanical and tribological behavior of Reinforced magnesium-based composite developed Via Friction stir processing. Proc Inst Mech Eng Part E J Process Mech Eng. 2021
2. Moustafa EB, AbuShanab WS, Ghandourah E, Taha MA. Microstructural, mechanical and thermal properties evaluation of AA6061/Al2O3-BN hybrid and mono nanocomposite surface. J Mater Res Technol [Internet]. 2020;9(6):15486–95. Available from: https://doi.org/10.1016/j.jmrt.2020.11.010
3. Cole GS. Summary of "Magnesium Vision 2020: A North American Automotive Strategic Vision for Magnesium." Essent Readings Magnes Technol. 2014; 9781118858943:35–40.
4. Han D, Zhang J, Huang J, Lian Y, He G. A review on ignition mechanisms and characteristics of magnesium alloys. J Magnes Alloy. 2020;8(2):329–44.
5. Esmaily M., J.E. Svensson, S. Fajardo, N. Birbilis, G.S. Frankel, S. Virtanen,R. Arrabal, S. Thomas, L.G. Johansson, Fundamentals and advances in magnesium alloy corrosion,Progress in Materials Science,Volume 89,2017,Pages 92-193,ISSN 0079-6425, https://doi.org/10.1016/j.pmatsci.2017.04.011
6. Peron M, Torgersen J, Berto F (2017) Mg and its alloys for biomedical applications: Exploring corrosion and its interplay with mechanical failure. Metals (Basel) 7.
7. Moustafa EB (2021) Hybridization effect of bn and al2o3 nanoparticles on the physical, wear, and electrical properties of aluminum aa1060 nanocomposites. Appl Phys A 127(9):1–9.
8. AbuShanab WS, Moustafa EB (2020) Effects of friction stir processing parameters on the wear resistance and mechanical properties of fabricated metal matrix nanocomposites (mmncs) surface. J Mater Res Technol 9(4):7460–7471.
9. Gupta M, Wong WLE. Magnesium-based nanocomposites: Lightweight materials of the future. Mater Charact [Internet]. 2015;105:30–46. Available from: http://dx.doi.org/10.1016/j.matchar.2015.04.015
10. Ghasali E, Alizadeh M, Niazmand M, Ebadzadeh T. Fabrication of magnesium-boron carbide metal matrix composite by powder metallurgy route: Comparison between microwave and spark plasma sintering. J Alloys Compd [Internet]. 2017;697:200–7. Available from: http://dx.doi.org/10.1016/j.jallcom.2016.12.146

11. Viswanath A, Dieringa H, Ajith Kumar KK, Pillai UTS, Pai BC. Investigation on mechanical properties and creep behavior of stir cast AZ91-SiCp composites. J Magnes Alloy [Internet]. 2015;3(1):16–22. Available from: http://dx.doi.org/10.1016/j.jma.2015.01.001
12. Bahrami A, Soltani N, Pech-Canul MI, Gutiérrez CA. Development of metal-matrix composites from industrial/agricultural waste materials and their derivatives. Crit Rev Environ Sci Technol. 2016;46(2):143–207.
13. Nguyen QB, Sharon Nai ML, Nguyen AS, Seetharaman S, Wai Leong EW, Gupta M. Synthesis and properties of light weight magnesium-cenosphere composite. Mater Sci Technol (United Kingdom) [Internet]. 2016;32(9):923–9. Available from: http://dx.doi.org/10.1080/02670836.2015.1104017
14. Kondaiah V V., Pavanteja P, Afzal Khan P, Anannd Kumar S, Dumpala R, Ratna Sunil B. Microstructure, hardness and wear behavior of AZ31 Mg alloy - Fly ash composites produced by friction stir processing. Mater Today Proc [Internet]. 2017;4(6):6671–7. Available from: http://dx.doi.org/10.1016/j.matpr.2017.06.441
15. Kumar H, Prasad R, Kumar P, Tewari SP, Singh JK. Mechanical and tribological characterization of industrial wastes reinforced aluminum alloy composites fabricated via friction stir processing. J Alloys Compd [Internet]. 2020;831:154832. Available from: https://doi.org/10.1016/j.jallcom.2020.154832
16. B. Ratna Sunil , G.P.K. Reddy , H. Patle , R. Dumpala , J. Magnes. Alloys 4 (2016) 52–61
17. Sharma V, Prakash U, Kumar BVM. Surface composites by friction stir processing: A review. J Mater Process Technol [Internet]. 2015;224:117–34. Available from: http://dx.doi.org/10.1016/j.jmatprotec.2015.04.019
18. Sagar P, Handa A (2020) Role of tool rotational speed on the tribological characteristics of magnesium based AZ61A/TiC composite developed via friction stir processing route. J Achiev Mater Manuf Eng 101:60–75.
19. Lu D, Jiang Y, Zhou R. Wear performance of nano-Al2O3 particles and CNTs reinforced magnesium matrix composites by friction stir processing. Wear [Internet]. 2013;305(1–2):286–90. Available from: http://dx.doi.org/10.1016/j.wear.2012.11.079
20. Yedla SB, Kalukanimuttam M, Winter RM, Khanna SK. Effect of shape of the tip in determining interphase properties in fiber reinforced plastic composites using nanoindentation. J Eng Mater Technol. 2008;130(4):0410101–04101015.
21. Krishnan KN. On the formation of onion rings in friction stir welds. Mater Sci Eng A. 2002;327(2):246–51.
22. Peng, J., Zhang, Z., Liu, Z. et al. The effect of texture and grain size on improving the mechanical properties of Mg-Al-Zn alloys by friction stir processing. Sci Rep 8, 4196 (2018). https://doi.org/10.1038/s41598-018-22344-3
23. Yadav, Devinder & Bauri, Ranjit. (2012). Effect of friction stir processing on microstructure and mechanical properties of aluminium. Materials Science and Engineering: A. 539. 85–92. 10.1016/j.msea.2012.01.055.
24. Sathiskumar R, Dinaharan I, Murugan N, et al. Influence of tool rotational speed on microstructure and sliding wear behavior of Cu/B4C surface composite synthesized by friction stir processing. Trans Nonferrous Met Soc China (English Ed.) 2015; 25: 95–102.
25. AMRA, M., RANJBAR, K., & HOSSEINI, S. A. (2018). Microstructure and wear performance of Al5083/CeO 2 /SiC mono and hybrid surface composites fabricated by

friction stir processing. Transactions of Nonferrous Metals Society of China, 28(5), 866–878. doi:10.1016/s1003-6326(18)64720-x
26. Prater T. Solid-state joining of metal matrix composites: A survey of challenges and potential solutions. Mater Manuf Process. 2011;26(4):636–48.
27. Hansen N. Hall-petch relation and boundary strengthening. Scr Mater. 2004;51(8 SPEC. ISS.):801–6.
28. Thangarasu, A., Murugan, N., Dinaharan, I. and Vijay, S.J. (2014), "Effect of tool rotational speed on microstructure and microhardness of AA6082/TiC surface composites using friction stir processing", Applied Mechanics and Materials, Vol. 592-594, pp. 234-239, doi: 10.4028/www.scientific.net/ AMM.592-594.234
29. LIU Q, KE L, LIU F, HUANG C, XING L. Microstructure and mechanical property of multi-walled carbon nanotubes reinforced aluminum matrix composites fabricated by friction stir processing [J]. Materials & Design, 2013, 45: 343−348.
30. Park SHC, Sato Y S and KokawaH2003 Effect of micro-texture on fracture location in friction stir weld ofMgalloy AZ61 during tensile test Scr. Mater. 49 161–6
31. Abbasi M, Bagheri B, Dadaei M, et al. The effect of FSP on mechanical, tribological, and corrosion behavior of composite layer developed on magnesium AZ91 alloy surface. Int J Adv Manuf Technol 2015; 77: 2051–2058.
32. Swedlow, J.L. On Griffith's theory of fracture. Int J Fract 1, 210–216 (1965). https://doi.org/10.1007/BF00186856
33. Sun, S.-J.; Kim, J.-S.; Lee, W.G.; Lim, J.-Y.; Go, Y.; Kim, Y.M.(2017) Influence of Friction Stir Welding on Mechanical Properties of Butt Joints of AZ61 Magnesium Alloy. Adv. Mater. Sci. Eng. 2017, 2017, 7381403.
34. Song X, Bayati P, Gupta M, Elahinia M, Haghshenas M. Fracture of magnesium matrix nanocomposites - A review. Int J Light Mater Manuf [Internet]. 2021;4(1):67–98. Available from: https://doi.org/10.1016/j.ijlmm.2020.07.002
35. Sahoo BN and Panigrahi SK2016 Synthesis, characterization and mechanical properties of in situ (TiC-TiB2) reinforced magnesium matrix composite Mater. Des. 109 300–13
36. Sharma S R,Ma Z Y and Mishra R S 2004 Effect of friction stir processing on fatigue behavior of A356 alloy Scr. Mater. 51 237–41
37. Niu PF, Tian BL. Wear Compensation Model Based on the Theory of Archard and Definite Integral Method. Math Probl Eng. 2018;2018.
38. Madhusudhan Reddy G, Sambasiva Rao A and Srinivasa Rao K. Friction stir processing for enhancement of wear resistance of ZM21 magnesium alloy. Trans Indian Inst Met 2013; 66: 13–24.
39. Sarmadi H, Kokabi AH and Seyed Reihani SM. Friction and wear performance of copper-graphite surface composites fabricated by friction stir processing (FSP). Wear [Internet] 2013; 304: 1–12.

Supplementary Table 1: Chemical composition of Magnesium base AZ31B alloy (EDS result).

Element	Aluminum, Al	Zinc Zn	Manganese Mn	Copper Cu	Calcium Ca	Iron Fe	Nickel Ni	Magnesium Mg	Silicon Si
Content (%)	3.4	1.5	0.2	0.05	0.04	0.005	0.005	88.1	6.7

Supplementary Table 2: Various technical properties of secondary phase **n-TiC** particulates

Purity (%)	Color	Average Particle Size (nm)	Specific Surface Area (m^2/g)	Bulk Density (g/cm3)	True Density (g/cm3)	Melting Point (°C)	Zeta Potential (mV)	Morphology
99	Black	80(Approx)	51	0.07	4.3	3190	2448	nearly spherical

Table 1: Average grain size and micro-hardness values of as-received and synthesized materials.

Test parameters	Base Matrix	Mono AZ31B/FA composite	Mono AZ31B/TiC composite	Hybrid AZ31B/TiC/FA composite
Vickers's Hardness (Hv)	55	80.1	89.2	95.1
Average grain size (μm)	78	5.4	4.9	3.8
Nano-hardness (GPa)	0.553	0.876	0.981	1.102

Table 2: Tensile tests results

Materials	E (GPa)	0.2%YS (MPa)	UTS (MPa)
Hybrid AZ31B/TiC/FA composite	7.97± 0.2	49.37 ± 2.5	204.8 ± 2.2
Mono AZ31B/TiC composite	6.16± 0.1	51.68 ± 3.2	128.0 ± 4.2
Mono AZ31B/FA composite	6.9± 0.3	53.32 ± 2.2	114.1 ±3.3
Base AZ31B Alloy	4.06 ±0.3	55.3 ± 2.2	84.37 ± 3.7

Table 3: Compressive test results

Materials	E (GPa)	0.2%CYS (MPa)	UCS (MPa)
Hybrid AZ31B/TiC/FA composite	11.36± 3.2	159.37 ± 2.3	232.22 ± 2.6
Mono AZ31B/TiC composite	10.16± 2.1	117.68 ± 4.5	175.55 ± 3.2
Mono AZ31B/FA composite	9.91± 4.3	118.32 ± 3.7	174.44 ±5.3
Base AZ31B Alloy	6.23 ±2.7	75.3 ± 3.8	128.88 ± 1.5

Supplementary Table 3: Wear properties of the base and developed composites

Component	Hybrid AZ31B/TiC/FA composite	Mono AZ31B/FA composite	Mono AZ31B/TiC composite	Base AZ31B Alloy
Wear rate (mm3/m)	0.011361	0.013499	0.012683	0.014068
Coefficient of friction	0.268	0.278	0.280	0.305

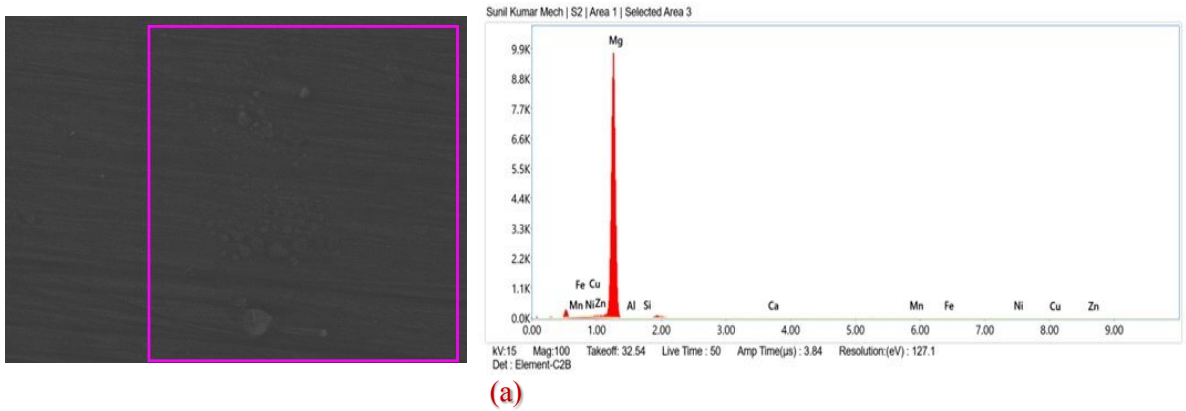

(a)

(b)

Supplementary Figure 1: AZ31B a) FESEM and EDS analysis b) AZ31B plate with blind holes

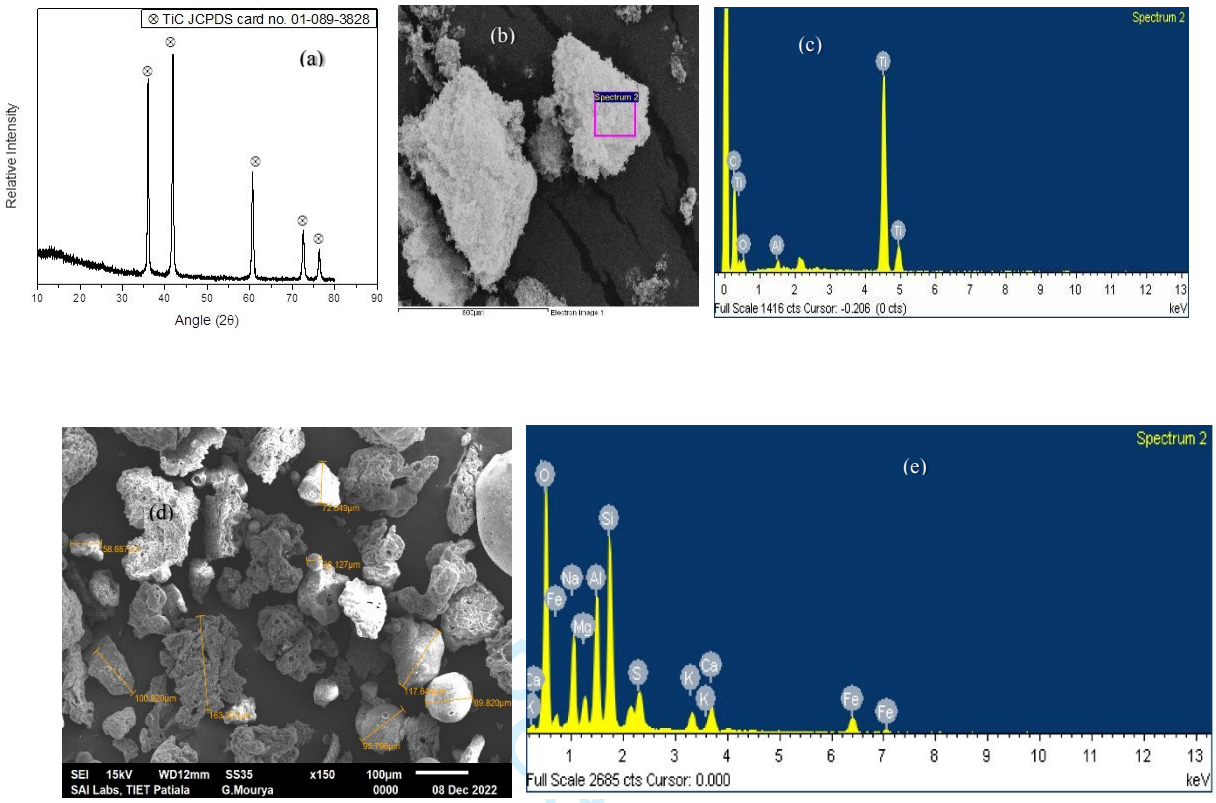

Supplementary Figure 2: TiC reinforcement a) XRD pattern b) FESEM results c) EDS results: FA d) SEM analysis and e) EDS spectrum results

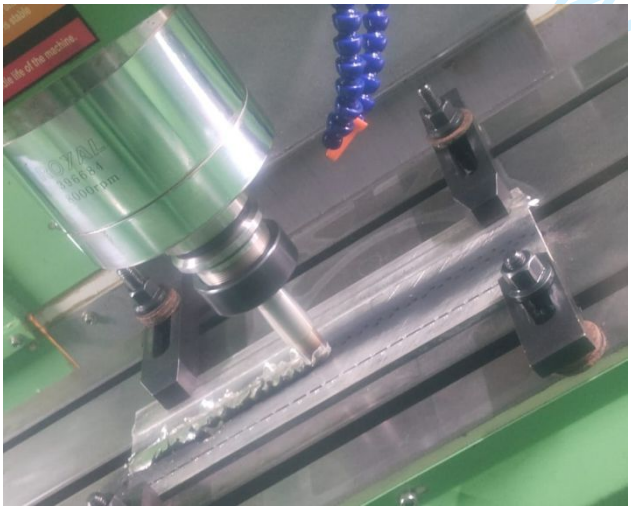

Supplementary Figure 3: Fabrication process of hybrid surface nanocomposite using FSP

Supplementary Figure 4: The FSP tools used for the manufacture of the composites.

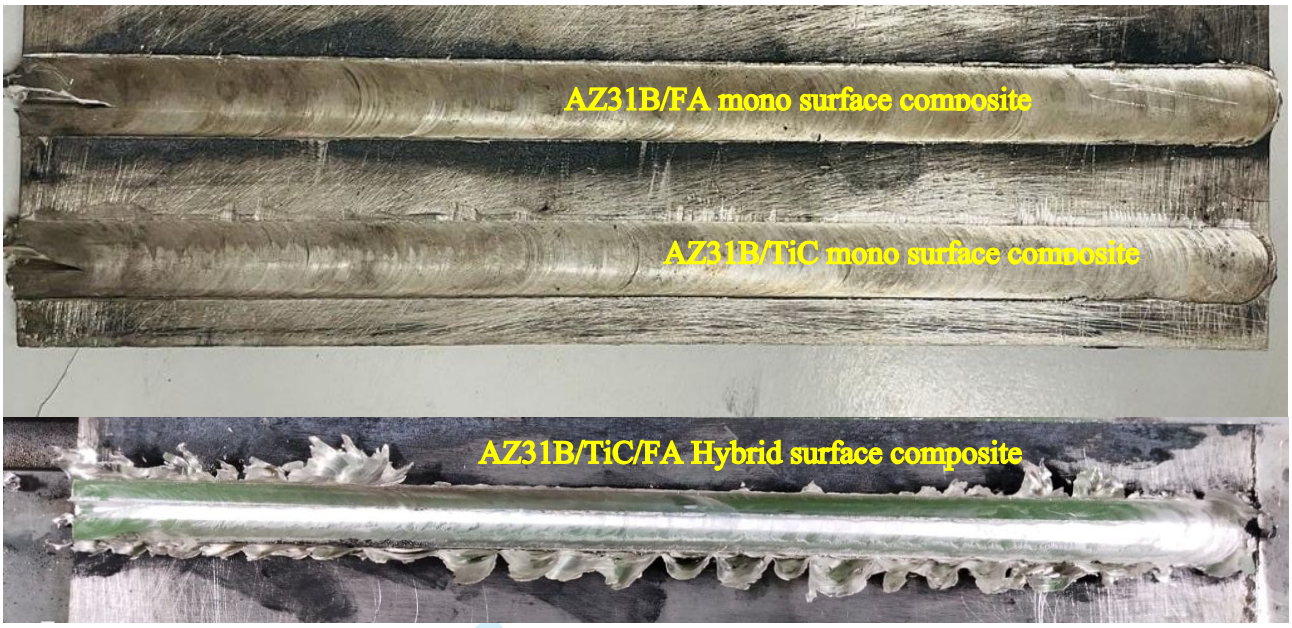

Supplementary Figure 5: Onion ring profile view of hybrid and mono composite surface after FSP process

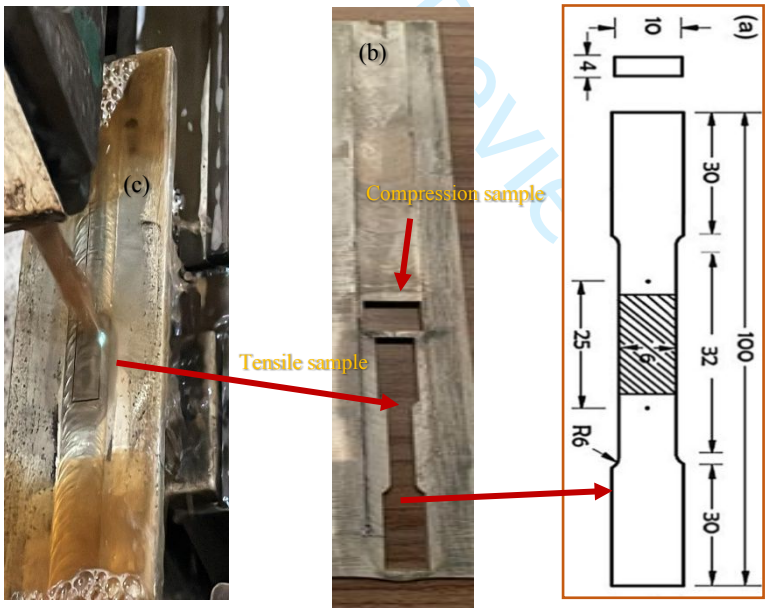

Supplementary Figure 6. a) Detailed geometry of tensile specimen: b) photograph of the actual specimen for tensile test: c) extraction of tensile specimen from stir zone using WEDM

Supplementary Figure 7: Extracted pins for wear examination

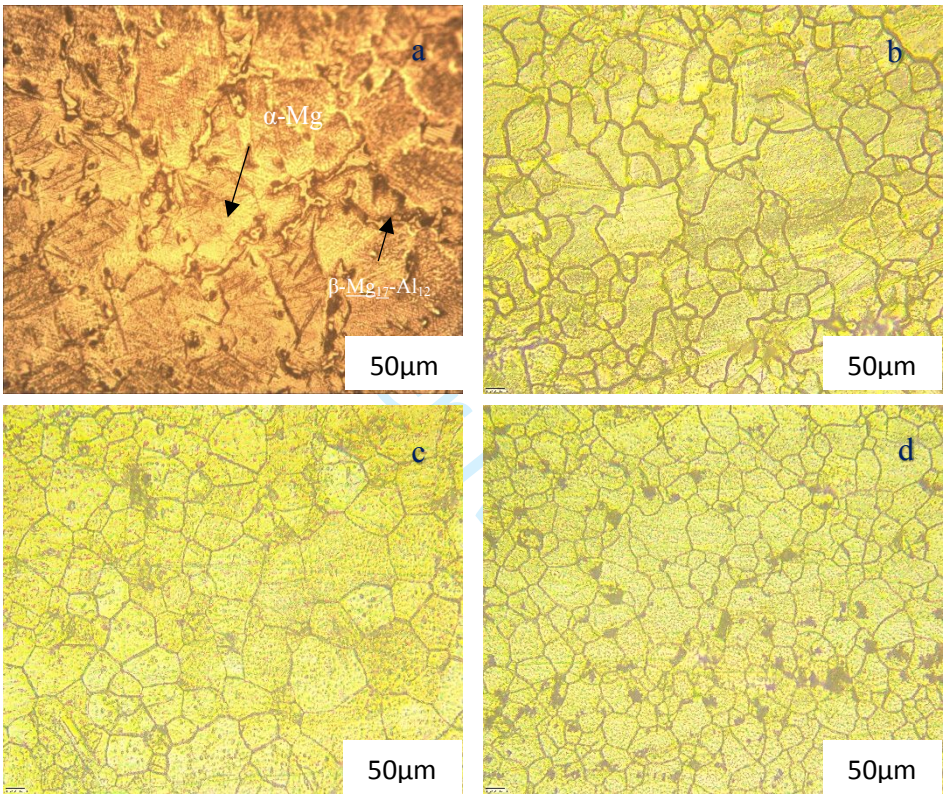

Figure 1: Microstructural images of a) base meatal: b) mono AZ31B/FA composite: c) mono AZ31B/TiC composite: d) hybrid AZ31B/TiC/FA composite captured from stir zone

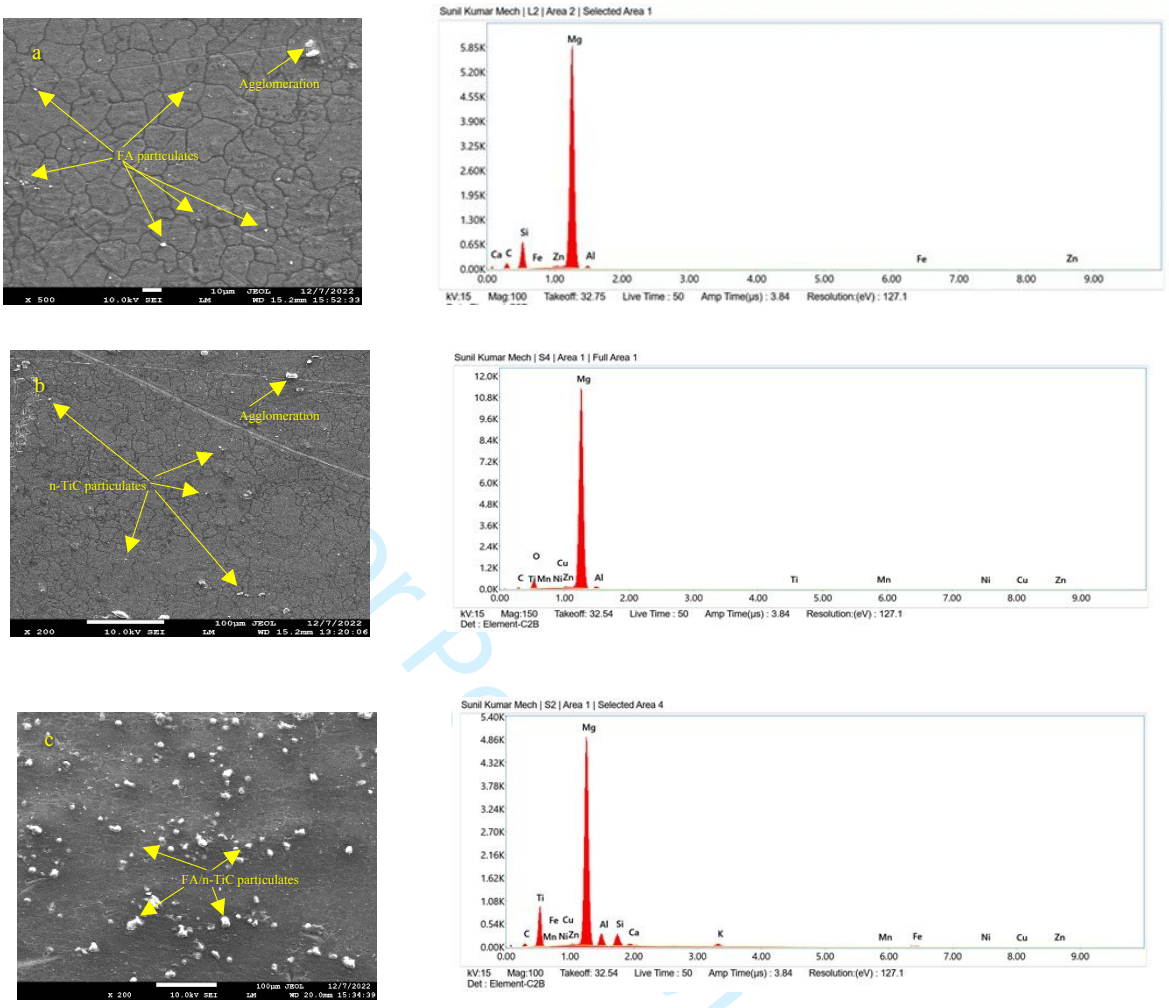

Figure 2: FESEM-EDS spectrum for the stir zone of a) mono composite AZ31B/FA b) mono composite AZ31B/TiC c) hybrid composite AZ31B/FA/TiC

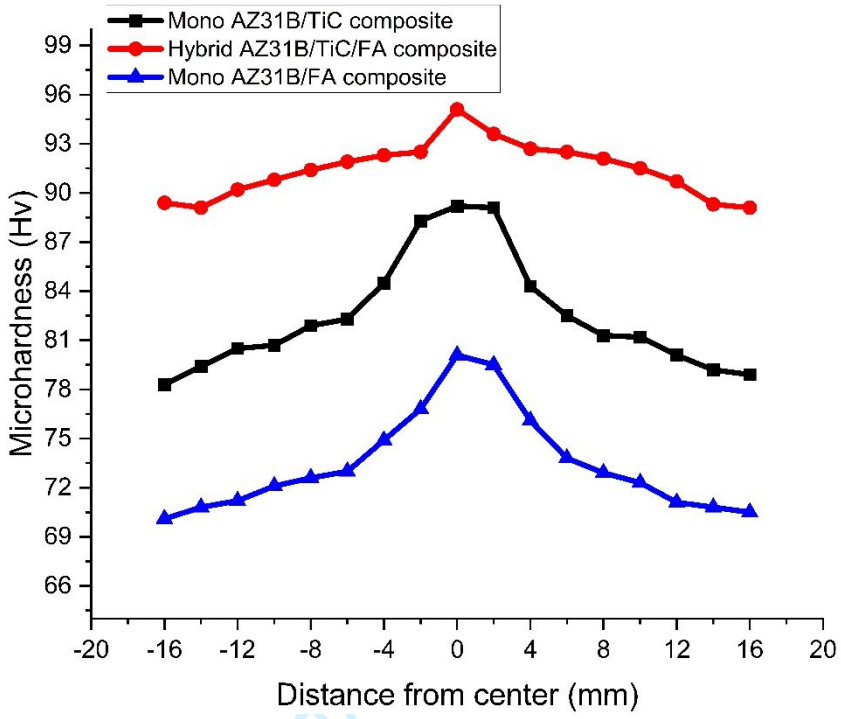

Figure 3: Micro hardness values for mono and hybrid composites

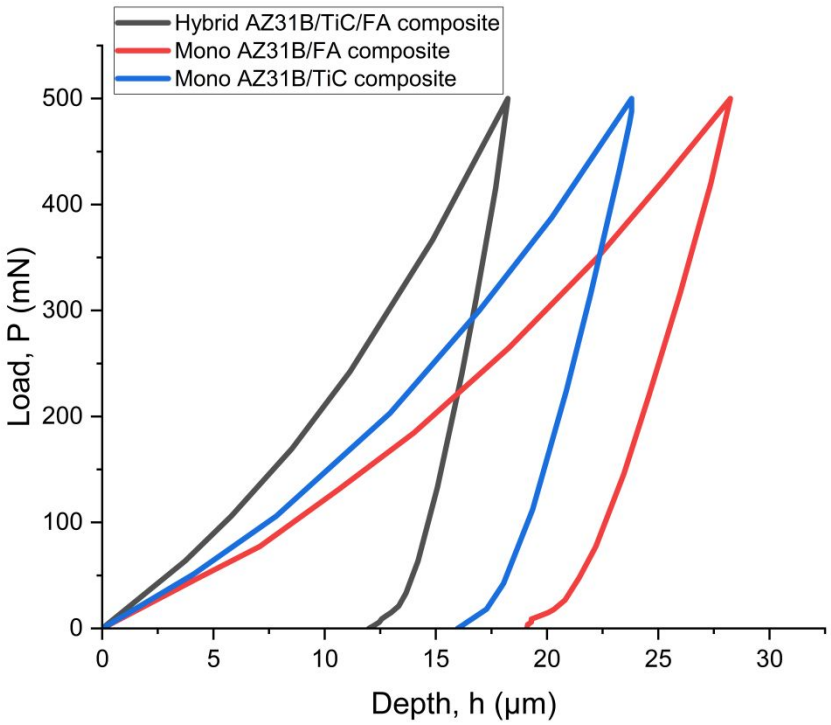

Figure 4: Load-displacement (P-h) curves of Nano-hardness experiments

Supplementary Figure 8: Tensile specimen before and after tensile testing

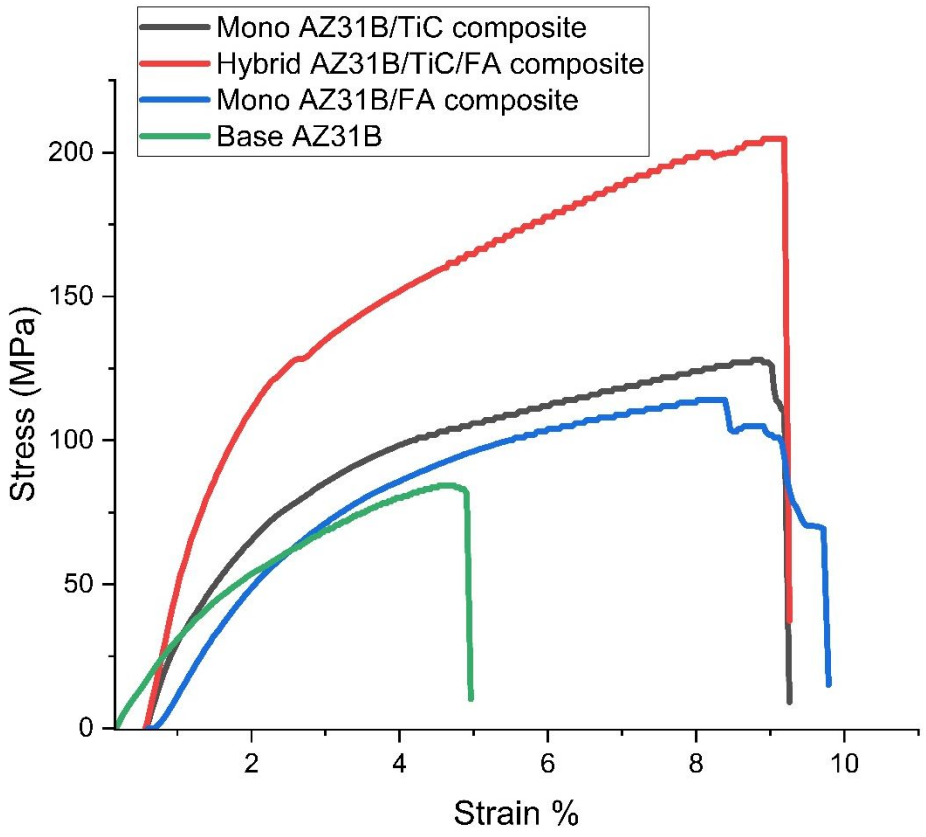

Figure 5: Tensile test stress-strain graphs of base Mg alloy and the composites

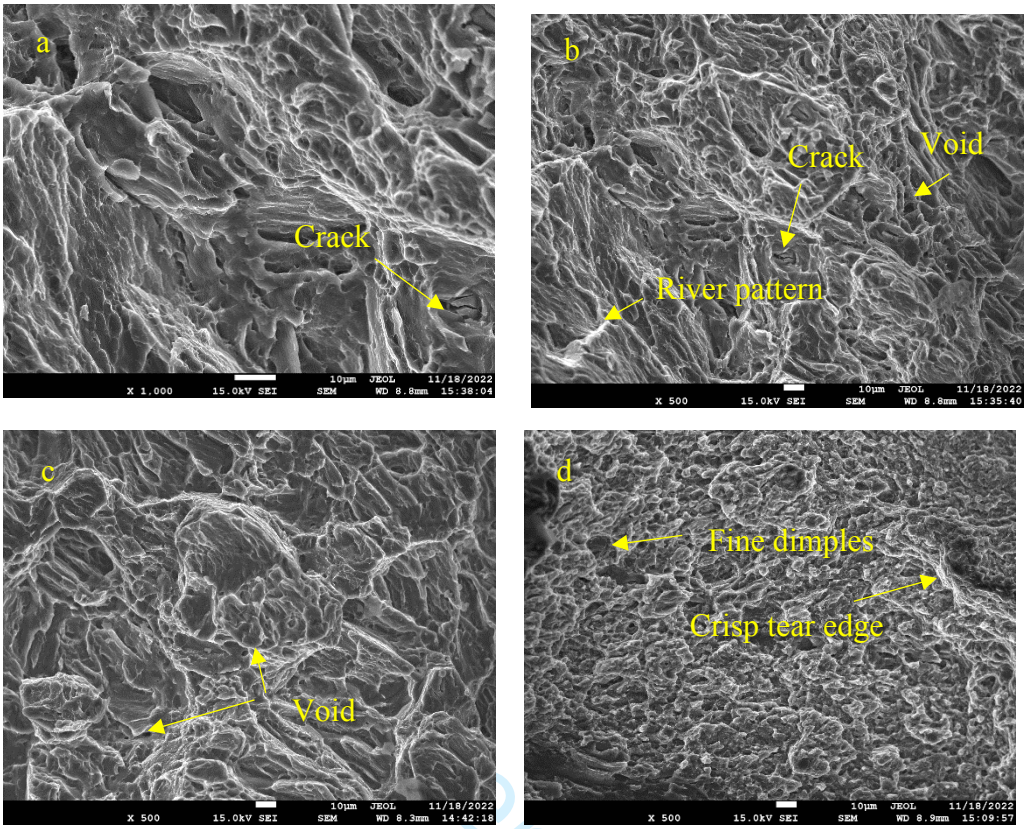

Figure 6: Tensile test SEM fractographs of a) base meatal: b) mono AZ31B/FA composite: c) mono AZ31B/TiC composite: d) hybrid AZ31B/TiC/FA composite

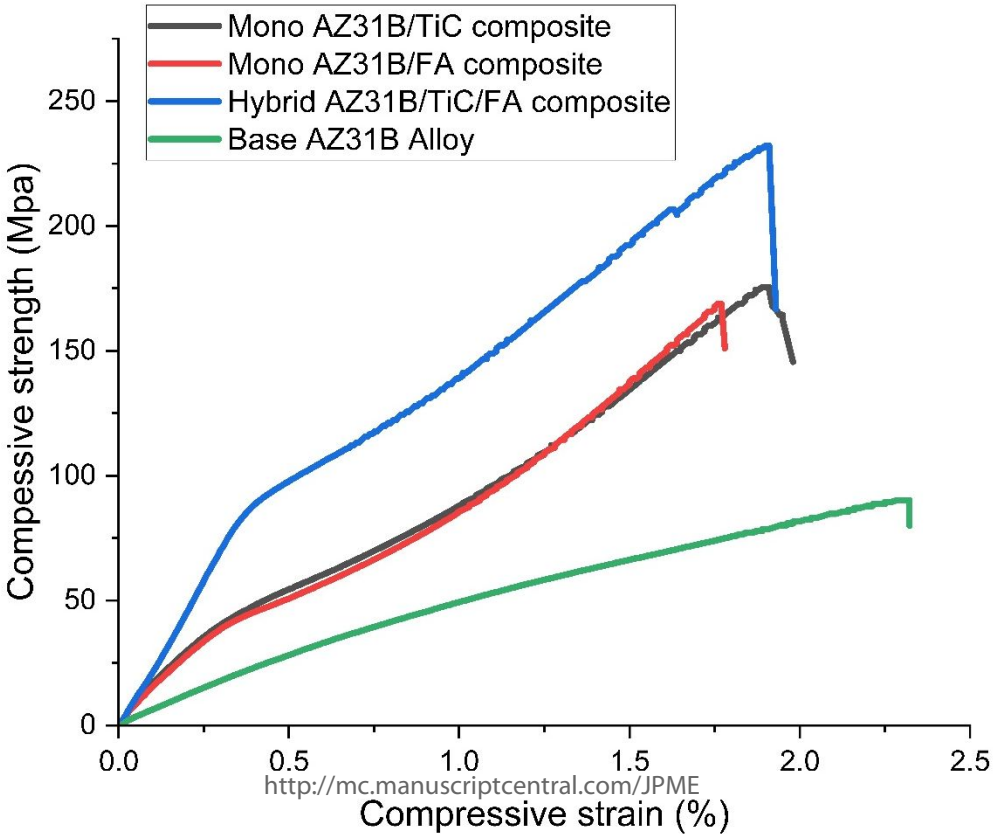

Figure 7: Compression test stress – strain curves for the base Mg alloy and the composites

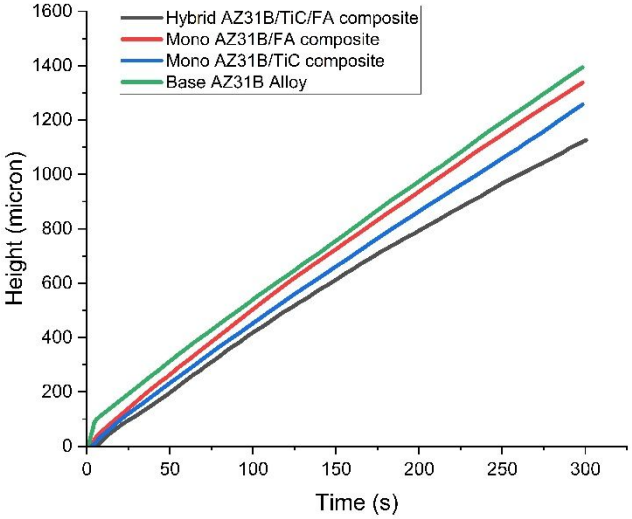

Supplementary Figure 9: Height loss of base, mono and hybrid composite during sliding wear test.

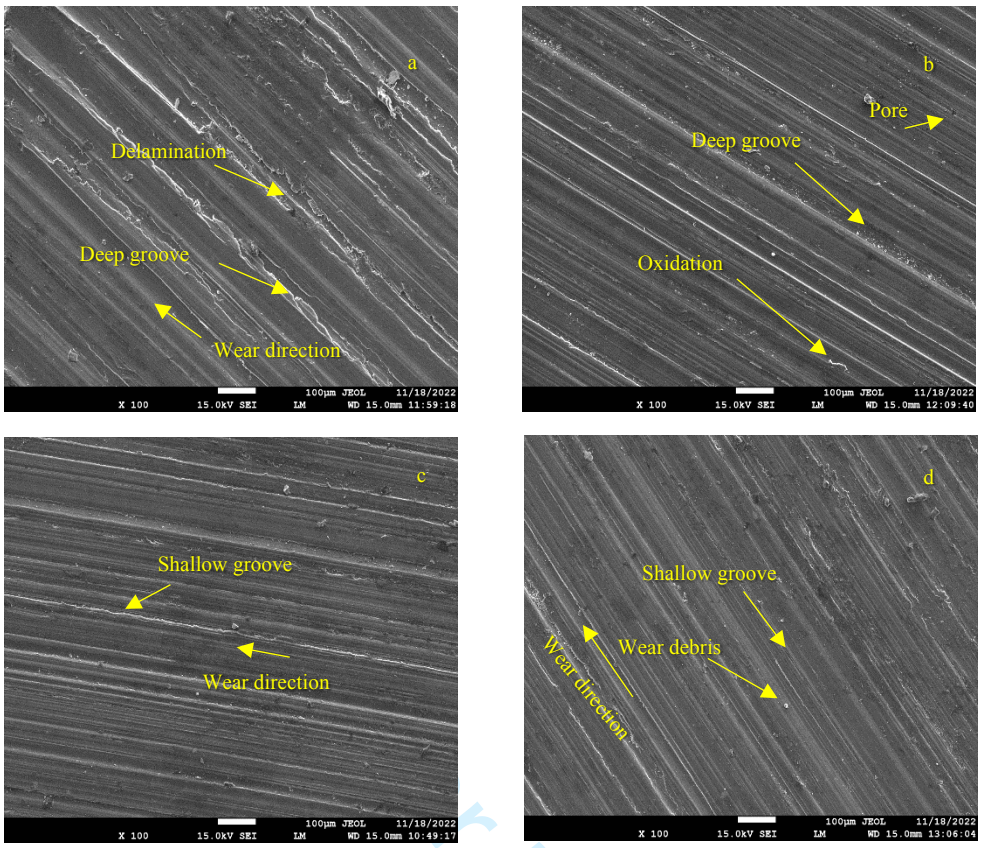

Supplementary Figure 10: Wear morphology of a) base meatal: b) mono AZ31B/FA composite: c) mono AZ31B/TiC composite: d) hybrid AZ31B/TiC/FA composite.